Malaysian Journal of Catalysis
http://mjcat.utm.my/
MJCat Research Article

Flake-like Tea-leaf-templated Magnesium Oxide for Carbon Dioxide Adsorption

Amirul Hafiiz Ruhaimi[1], Mohd Rozainee Taib[1] and Muhammad Arif Ab Aziz[1,2]*,

[1] *School of Chemical and Energy Engineering, Faculty of Engineering, Universiti Teknologi Malaysia (UTM), 81310 UTM Johor Bahru, Johor, Malaysia*
[2] *Centre of Hydrogen Energy, Institute of Future Energy, Universiti Teknologi Malaysia (UTM), 81310 UTM Johor Bahru, Johor, Malaysia*

**Corresponding Author: m.arif@utm.my*

Article history:
Received 16 February 2022
Accepted 5 April 2022

GRAPHICAL ABSTRACT

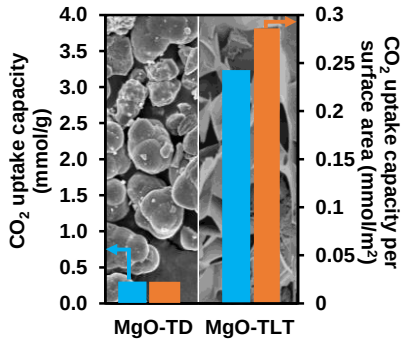

ABSTRACT

Flake-like mesoporous magnesium oxide (MgO-TLT) was prepared using a bio-templating method with tea leaves (TLTs) as the template. MgO-TLT exhibited smaller crystallites (7.52 nm) than MgO prepared using the thermal decomposition method (22.52 nm). These smaller crystallites led to more structural defects in the adsorbent and a high basic site density; consequently, MgO-TLT exhibited a high CO_2-uptake capacity of 3.17 mmol/g, which is 12-times higher than that of MgO-TD at 1 atm and 300 K, despite its low surface area. Furthermore, based on its low surface area and high uptake capacity, MgO-TLT has an uptake capacity per surface area that is more than 15-times higher than that of MgO-TD, which supports the hypothesis that MgO-TLT possesses more surface defect sites that promote the attachment of CO_2. This study revealed that TLT is a promising template for use in the bio-templating syntheses of MgO adsorbents with high surface reactivities and enhanced CO_2-uptake capacities.

Keywords: Mesoporous magnesium oxide, CO_2 adsorption, bio-templating, spend tea leaves

| eISSN 0128-2581 |

1. INTRODUCTION

Increasing concentrations of atmospheric CO_2 have attracted considerable attention owing to their long-term destructive impacts on the environment and climate. Increasing CO_2 concentrations are mainly due to uncontrolled greenhouse gas emissions from industries that consume fossil fuels [1]. Hence, several approaches for minimising CO_2 released into the atmosphere have been proposed and investigated, including carbon-capture technology. Adsorption techniques have progressively been studied as replacements for the currently widely used CO_2-capture technique that has several drawbacks, such as a high absorbent make-up rates, high energy consumption during the regeneration process [2], flow problems [3], high rates of equipment corrosion due to the formation of acidic chemicals, the loss of amines due to the presence of SO_2, NO_2, and O_2, and evaporation [4, 5]. On the other hand, adsorption is a superior technique in terms of cost efficiency, facile operational conditions, environmental friendliness, and recyclability [6].

A number of adsorption techniques that use metal-oxide-based adsorbents have been studied with the aim of identifying the structural properties required to achieve high CO_2-uptake capacities. Theoretically, a metal-oxide adsorbent, such as MgO, has a high uptake capacity for CO_2 of around 24.8 mmol/g [7]. However, the poor structural properties of common MgO, including its low adsorbent surface area and surface basicity, result in a low CO_2-uptake capacity because CO_2 cannot effectively access the active sites of the adsorbent [8]. While numerous studies aimed at improving the structural properties of adsorbents have been reported, current high-surface-area synthesis methods that use surfactants, such as cetyltrimethylammonium-bromide (CTAB), as templates, are costly because surfactant templates are expensive and the synthesis procedures are complex [9, 10]. Therefore, using a biomass-based (biomaterial-based) template represents an attractive alternative approach because such biomaterial templates can

generate adsorbents with unique structural and textural properties.

A number of studies have been documented benefiting from the bio-templating approach in various applications. For instances, by using cotton [11-13], Arabic gums [14], palm olein [15], paper fibre [16], rose petal [17-19], eggshell membrane [6, 20, 21], citrus peel [22, 23], etc… The prepared material obtained from the bio-templating method has demonstrated decent physicochemical properties in term of surface area and surface reactivity, which improved the performance, in particular for CO_2 adsorption application [6, 20, 22]. With this background in mind, the author has considered utilising the spent tea leaves as a biomaterial template in this CO_2 capture application. Due to highly consumed drinks worldwide with 18 – 20 billion cups of tea daily, plenty of spent tea leaves was generated from industry and households that were released into the environment as waste without any economic value [24]. Thus, beneficiation of the spent tea leaves (STL) is highly desired. Accordingly, to date number of studies have been conducted utilising STL in several applications, such as in the separation process, particularly as the main component or as an enhancement supporting material [24-27]. The consideration of utilising STL in addition to highly-available sources might possibly be on account of the STL's morphology features; it is reported possessing a diversified, coarse and highly porous surface composed of numerous fibrous bonds and spongy formations [28]. This could result in the final STL-used material with decent textural properties, which further influenced the performance.

Hence, in this study we fabricated a MgO adsorbent using tea leaves (TLTs) as the biomaterial template. Moreover, we also synthesised a MgO adsorbent using the thermal decomposition (TD) method and compared the physicochemical properties and uptake capacities of the MgO-TLT and MgO-TD adsorbents using FESEM, XRD, N_2 physisorption, FTIR-KBr, and TGA characterisation techniques. The CO_2-uptake capacities of the prepared adsorbents were investigated using flowing pure CO_2 at ambient pressure and temperature.

2. EXPERIMENTS

2.1 Adsorbent preparation

TLT bio-templating was initiated by immersing TLTs in boiling water several times to remove any colour residue remaining in the TLTs. The filtered TLTs were then placed in a beaker and dried overnight at 383 K. Mg $(NO_3)_2{\cdot}6H_2O$ (20 g; QRëC, 99.5%) was dissolved in ethylene glycol (EG) (200 mL; QRëC, 99.5%) with stirring and then sonicated for 10 min. Dried TLTs (5 g) were then immersed in the solution and stirred for 1 h at room temperature. Aqueous ammonia solution (5 mL, QRëC, 28%) was then added, with stirring continued for another 30 min. The TLT adsorbent was then collected by filtration, dried for 1 h at 373 K, and calcined at 823 K for 3 h. The prepared adsorbent is referred to as "MgO–TLT". MgO-TD was prepared by preheating Mg $(NO_3)_2{\cdot}6H_2O$ at 373 K for 1 h after which it was calcined at 823 K for 3 h.

2.2 Characterising the adsorbent and examining its CO_2 adsorption properties

Each adsorbent was subjected to FESEM (ZEISS Crossbeam 340) to examine its morphology, and XRD (Rigaku SmartLab with Cu Kα radiation) in the 2–90° 2θ range to investigate its crystallinity. Average adsorbent crystal size was calculated using the high-intensity XRD peak and Scherrer's equation. Textural properties were evaluated by acquiring N_2-adsorption/desorption isotherms with a gas-sorption analyser (Quantachrome Instruments, Autosorb IQ, version 3.0) after pre-treating the sample at 523 K; the obtained data were analysed using 3Flex software (version 5.0). FTIR spectra of the adsorbents were obtained on a Cary 600 series spectrometer in the 400–4000 cm^{-1} range, and the prepared adsorbents were subjected to TGA in the 303–1173 K temperature range at 10 K/min under a flow of N_2 gas. Each prepared adsorbent was examined for its CO_2 uptake capacity during CO_2-adsorption testing using a fixed-bed U-shaped gas column equipped with a CO_2 analyser under a flow of pure CO_2 at 1 atm and 298 K.

3. RESULTS AND DISCUSSION

The FESEM images in Figure 1 show that the prepared MgO samples exhibit different morphological features: MgO-TD has a spherical structure (Figure 1a) that is attributable to the direct conversion of the magnesium salt into MgO during calcination. In contrast, the TLT bio-templating method led to MgO with a thin flake-like structure (Figure 1b); this morphology is possibly associated with the use of ethylene glycol during preparation. Ethylene glycol is a promising chelating agent for polyols due to its two hydroxyl groups (-OH) [29, 30]. During synthesis, bonds can form between two or more binding sites with the same ethylene glycol ligand and a single central metal atom to form an intermediate metal-polyol complex [29] in a process known as "chelation". The following mechanism for the formation of the intermediate metal-polyol complex during $Mg(NO_3)_2$ dissolution in ethylene glycol is proposed:

$$(CH_2OH)_2 + Mg(NO_3)_2 \rightarrow Mg(OCH_2)_2 + 2HNO_3 \qquad (1).$$

As reported previously, the use of ethylene glycol and a Mg salt can result in the formation of magnesium ethylene glycolate, as an intermediate metal-polyol complex, which is then converted into MgO during calcination [6]. According to several studies, the use of a polyol (i.e., ethylene glycol) as the solvent for the MgO adsorbent results in the formation of flake-like or flower-like structures with

thin flake-like petal features or other similar structures [6, 30-32]; a flake-like structure was formed instead of a flower-like structure in this study, which is possibly be due to the attachment of magnesium ethylene glycolate to the TLT surface [30-32]. The thin flake-like structure exhibited by the MgO adsorbent is reportedly beneficial because it lowers the diffusion-resistance layer and improves MgO-use efficiency, which is expected to enhance the CO_2-adsorption performance of the adsorbent [33].

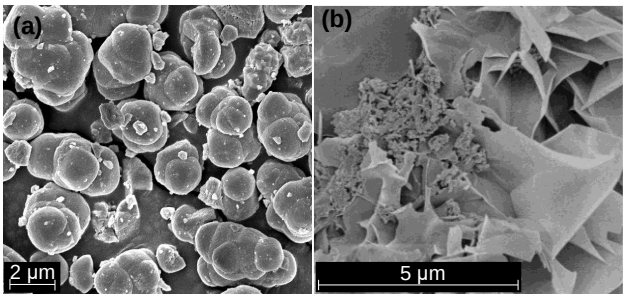

Figure 1. FESEM images of a) MgO-TD and b) MgO-TLT.

The XRD pattern of MgO-TD (Figure 2a) reveals a series of diffraction peaks at 2θ = 36.8°, 42.8°, 62.2°, 74.6°, and 78.6° that can be assigned to the (111), (200), (220), (311), and (222) crystal planes of the cubic fluorite MgO structure [34]. Moreover, MgO-TLT exhibits roughly the same diffraction peaks, although with significantly less intense; these weaker peaks are consistent with smaller crystallites. In addition, the (200) peak of MgO-TLT displayed a shifting to lower 2θ value, which indicates an expansion to a higher lattice parameter [35]. The average crystallite sizes of the prepared adsorbents were calculated using the Scherrer equation, with the (200) peak as a reference. MgO-TD was found to possess larger crystallites (19.30 nm) than MgO-TLT (4.94 nm); hence, we conclude that the use of TLT as a template produced an adsorbent with smaller crystallites than that prepared by the thermal decomposition method or previously reported bio-templated MgO (14.31 nm) [6]. On the other hand, through William-Hall (W-H) plotting (Figure 2b), where the crystallite size of both MgO-TD and MgO-TLT adsorbents are slightly different compared to Scherrer calculation, which 17.95 nm and 3.82 nm, respectively. Through W-H methodology, XRD peak broadening controlled by both size and the lattice strain could be appropriately expressed by Williamson–Hall equation (1) below [36]:

$$\frac{\beta cos\theta}{\lambda} = \frac{1}{D} + \eta \frac{sin\theta}{\lambda} \quad (1)$$

Where λ is the x-ray wavelength of the equipment used (0.1589), θ is the peak position (radians), η is an order of refraction, λ is the x-ray wavelength (0.1589), β is the line broadening at half maximum intensity (FWHM) (radians), D is the effective crystallite size (nm), and η is the effective strain. The y-intercept and the slope of the linear fitting indicate the effective crystallite size (1/D) and effective strain (η), respectively. As depicted in Figure 2b, both adsorbents exhibited a negative slope (strain, η), indicating a compressive strain (lattice shrinkage), whereas a positive slope is the signature of tensile strain [14, 37]. According to many reports, the negative slope is encountered when the crystallite size of the sample is small, less than 20 nm [38].

The difference in crystallite size obtained through the Scherrer method and W-H plotting is owing to the consideration of the lattice strain to the peak broadening.

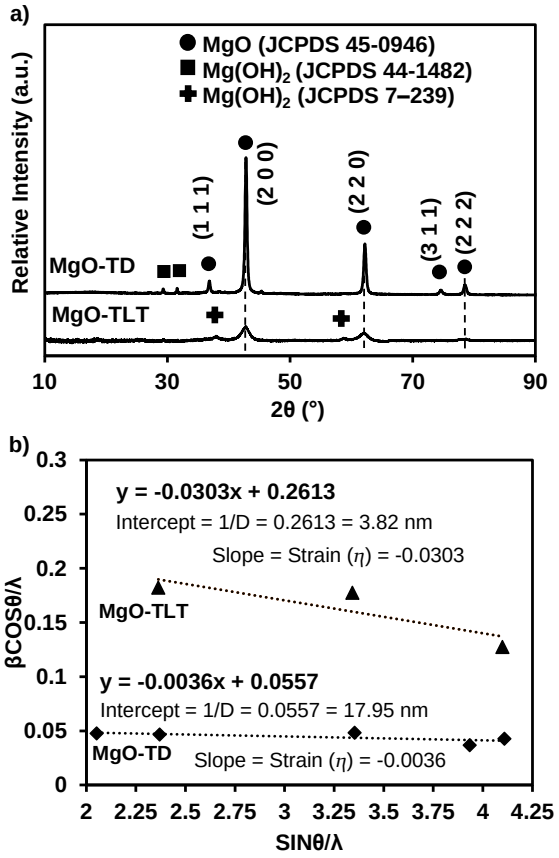

Figure 2. a) XRD patterns and b) Williamson-Hall (W–H) plot of the MgO adsorbent

Moreover, to further understand the nanocrystallite structure of the prepared adsorbent derived from the XRD profile, the estimation of lattice strain (ε) and dislocation density (δ) was performed. The effect of bio-templating on the dislocation density and strain of the prepared MgO was investigated using Eqs. (2) and (3), respectively, [39].

$$\delta = \frac{1}{D^2} \quad (2)$$

$$\varepsilon = \frac{\beta}{4 \tan \theta} \quad (3)$$

As presented in Table 1, MgO-TLT shows higher dislocation values and strain than MgO-TD, which inversely interdependence to the crystallite size. The reason for the high lattice strain of MgO-TLT is proposed to be the influence of grain boundary. According to Shafi and Bose, for the smaller size nanostructured material, a grain boundary is associated with more volume defects like vacancies and vacancy clusters [40]. Where the stress field results from the volume defects at the grain boundaries exert lattice strain in nanostructured materials. This is also influenced by the internal pressure exerted by the surface tension on the nanomaterial, which will create a stress field inducing a lattice strain.

Table 1. The estimation of the nano-structural parameters of prepared MgO.

Lattice planes	2θ (°)	β (°)	D(nm)*	δ x 10^{-3} (nm^{-2})	ε x 10^{-3}
MgO-TD					
(1 1 1)	36.85	0.44	18.92	2.79	5.80
(2 0 0)	42.83	0.44	19.30 (17.95)	2.68	4.92
(2 2 0)	62.22	0.50	18.67	2.87	3.59
(3 1 1)	74.60	0.41	24.58	1.65	2.33
(2 2 2)	78.55	0.49	21.07	2.25	2.60
Average				**2.45**	**3.85**
MgO-TLT					
(2 0 0)	42.70	1.73	4.94 (3.82)	40.98	19.27
(2 2 0)	61.97	1.83	5.07	38.87	13.27
(2 2 2)	78.33	1.45	7.06	20.04	7.77
Average				**33.30**	**13.44**

* : Scherrer calculation

Values in parenthesis are the estimation of crystallite size using W-H methodology

Based on the above discussed nano-structural parameter, it is believed that the smaller MgO-TD crystallite size was associated with the presence of a higher structural defect site in the adsorbent then promotes high CO_2 uptake capacity [41]. This finding was supported by a previously reported study, where the egg-shell membrane (ESM) bio-templating method has resulted in the MgO-ESM adsorbent with a smaller crystallite size than the conventional thermal conversion method [6]. Furthermore, through a CO_2-TPD analysis of the above-mentioned study, it is found that flake-shaped MgO-ESM with small crystallite size demonstrated much stronger surface basicity than thermally converted MgO. This is possibly contributed by the presence of high basic site density. Moreover, this MgO-TLT finding was also consistent with several related studies in which bio-templating methods reportedly resulted in smaller adsorbent crystallites [20, 22] that significantly improved the adsorption uptake capacity.

Figure 3 shows FTIR spectra of the MgO-TD and MgO-TLT adsorbents. Both adsorbents exhibit approximately the same transmittance bands in their spectra; those at 3692 and 3460 cm^{-1} are assigned to the stretching vibrations of hydroxyl groups on crystal faces with low-coordination or defect sites, and residual moisture, respectively [42, 43]. The acquired spectra show that MgO-TLT contains a large amount of moisture. Moreover, both adsorbents exhibit bands located at approximately 1640 cm^{-1} that is associated with the bending mode of the hydroxyl groups of adsorbed molecular water attached at hydroxide and magnesia surfaces of the adsorbents [44]. In addition, the strong band observed at 1418–1490 cm^{-1} in the spectrum of MgO-TLT is attributable to the asymmetric stretching vibrations of CO_3^{2-}, which is possibly associated with carbonate species formed on the adsorbent surface [45, 46]. MgO-TD also exhibited the same CO_3^{2-} band; however, this band is less intense than that observed for MgO-TLT. This indicates that MgO-TLT is able to adsorb (via chemisorption attachment) more CO_2 from the atmospheric surrounding than MgO-TD. This likelihood could possibly be influenced by the high surface reactivity of the adsorbent, which is promoted by the present rich surface defects, i.e. cationic vacancies site (Mg^{2+}) and low-coordination anionic sites (O^{2-}) on MgO-TLT [47]. In addition, the vibrational bands observed at 862 and 550 cm^{-1} are attributable to bonds in cubic MgO and the Mg-O-Mg stretching mode, respectively [48, 49].

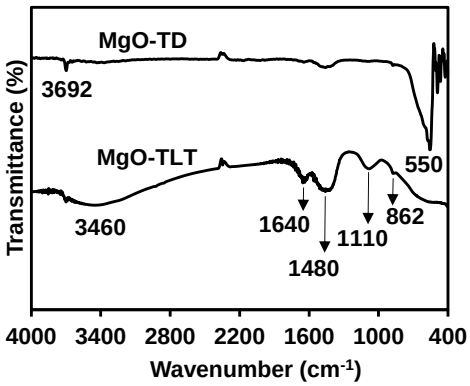

Figure 3. FTIR spectra of the prepared MgO adsorbents.

According to the N_2-adsorption–desorption isotherms, which are used to assess textural properties (Figure 4), both MgO adsorbents exhibit type-IV isotherms with H3-type hysteresis loops that indicate the presence of slit-shaped mesoporous structures [32]. MgO-TLT was found to have a slightly smaller BET surface area (11.27 m^2/g) than MgO-TD (13.63 m^2/g). This could possibly be associated with the

TLT bio-template material used, where TLT's morphological and surface functional features do not provide a significant role in the bio-templating approach. Unlike the previously studied ESM bio-templating approach, in which the interconnected fibrous network structure of the ESM with an abundant surface functional group has contributed to the enhancement of the bio-templated adsorbent structural properties [6, 20]. Moreover, the pore volume of MgO-TLT (0.007 cm^3/g) is also smaller than that of MgO-TD (0.06 cm^3/g). Although, it is worth noting that these inferior textural properties did not directly influence the CO_2 capture performance of the adsorbent. The presence of small average pore width of MgO-TLT with 6.4 nm is found beneficial for CO_2 uptake performance compared to MgO-TD with 17.5 nm. This could possibly be associated with the adsorbate-adsorbate (gas-gas) and adsorbate-adsorbent (gas-MgO) interaction. According to Ma et al., decreases in pore width will increase the CO_2 uptake densities of the adsorbent, in-which attributed to the strongly adsorbate-adsorbate and adsorbate-adsorbent interaction [50]. This consequently results in increasing adsorption heat which indicates the strong adsorption potential. Thus, improving the adsorbent's CO_2 capture.

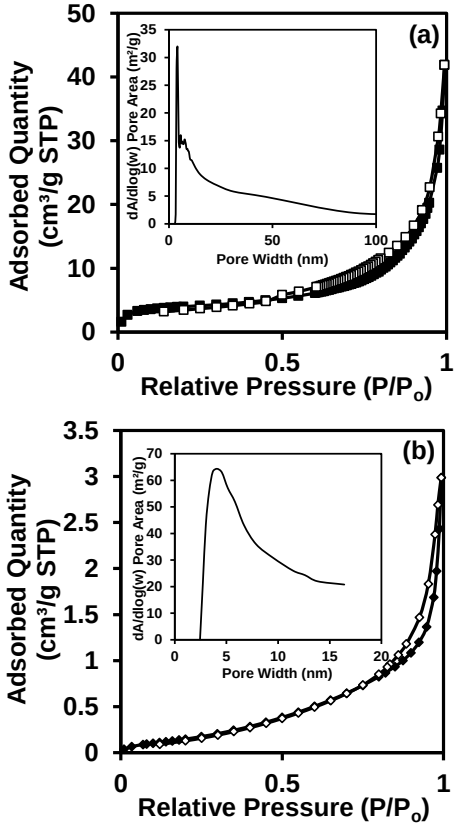

Figure 4. N_2-adsorption–desorption isotherms for a) MgO-TD and b) MgO-TLT. The insets show pore distribution curves.

As shown in Figure 5(a, b), MgO-TD and MgO-TLT exhibit very similar thermal decomposition pattern that includes three degradation stages, with water, organic compounds, and trapped carbonaceous residues removed in the first (< 513 K), second (513–773 K), and third stages (>773 K), respectively. Yet, the intensity of the weight loss is different, where the overall evaluation has shown that MgO-TD demonstrated more weight (38%) than MgO-TLT with 23%. This high weight loss observed for MgO-TD is possibly due to the large amount of organic residue present in the adsorbent, which is supported by an intense second-stage derivative weight-loss curve. Moreover, in the first and third stages, both MgO adsorbents have displayed a similar weight loss with a mostly similar derivative weight-loss curve.

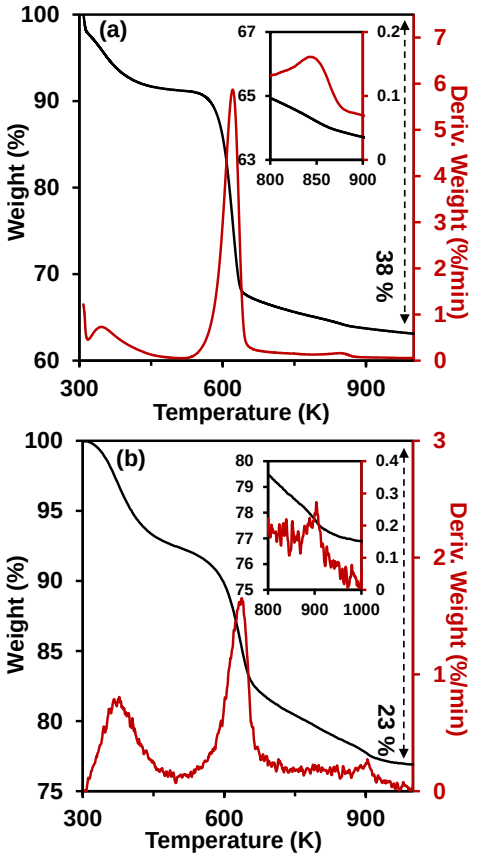

Figure 5. TGA profiles of a) MgO-TD and b) MgO-TLT. (Insert: Close-up scale of TGA profile of MgO-TD on the 3rd degradation stage)

CO_2-adsorption experiments were used to examine the association between the physicochemical properties and the CO_2-uptake capacity of each adsorbent. As depicted in Figure 6, MgO-TLT exhibited a significantly larger CO_2-uptake capacity (3.17 mmol/g) than MgO-TD (0.25 mmol/g), despite its low surface area. Moreover, the CO_2-uptake efficiency per surface area of MgO-TLT was determined to be around 0.28 $mmol/m^2$, which is almost 16-

times higher than that of MgO-TD, and it is possibly associated with superior physicochemical properties of MgO-TLT, as evidenced by the characterisation data presented above; small crystallite size and pore width. The smaller crystallites of MgO-TLT compared to those of MgO-TD (XRD section) may provide more structural defects in the adsorbent that result in a high basic site density [41]. This could also be supported by the presence of an intense band associated with adsorbed atmospheric CO_2 (FTIR section). Hence, we conclude that the TLT bio-templating method developed in this study resulted in the fabrication of MgO-TLT with significantly superior CO_2-uptake capacity despite its lower surface area.

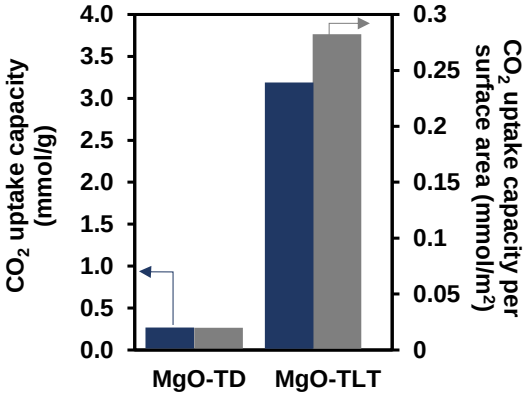

Figure 6. CO_2-uptake capacities of the MgO adsorbents.

4. CONCLUSION

In this study, we successfully synthesised mesoporous flake-like MgO-TLT using TLT as a template. TLT bio-templating resulted in the fabrication of MgO with a highly reactive surface, as evidenced by FTIR spectroscopy, which revealed bands that correspond to carbonate species formed by the attachment of atmospheric CO_2 to the MgO-TLT surface. In addition, despite its smaller surface area compared to that of MgO-TD, as well as several studies that report the same morphological features, MgO-TLT exhibited a high CO_2-uptake capacity of 3.17 mmol/g, which is 12-times higher than that of MgO-TD. Moreover, MgO-TLT also exhibited a high uptake capacity per surface area that is more than 15-times higher than that of MgO-TD and is ascribable to its high surface reactivity. Therefore, this study revealed that tea leaves are a promising and low-cost template source for the fabrication of MgO with a high CO_2-uptake capacity.

ACKNOWLEDGEMENTS

This work was supported by the Universiti Teknologi Malaysia (Grant No. 08G94) and the Ministry of Higher Education Malaysia through Fundamental Research Grant Scheme (FRGS) Grant No. FRGS/1/2019/STG07/UTM/02/8 (Grant No. 5F217).

REFERENCES

[1] J.D. Shakun, P.U. Clark, F. He, S.A. Marcott, A.C. Mix, Z. Liu, B. Otto-Bliesner, Nature 484(7392) (2012) 49.
[2] Q. Lai, Z. Diao, L. Kong, H. Adidharma, M. Fan, Appl. Energy 223 (2018) 293.
[3] A. Azmi, M. Aziz, J. Environ. Chem. Eng. 7(2) (2019) 103022.
[4] M. Aghaie, N. Rezaei, S. Zendehboudi, Renew. Sust. Energ. Rev. 96 (2018) 502.
[5] L. Jiang, A. Gonzalez-Diaz, J. Ling-Chin, A. Roskilly, A. Smallbone, Appl. Energy 245 (2019) 1.
[6] A.H. Ruhaimi, M.A. Ab Aziz, J. Solid State Chem. 300 (2021) 122242.
[7] W. Gao, T. Zhou, Y. Gao, B. Louis, D. O'Hare, Q. Wang, J. Energy Chem. 26(5) (2017) 830.
[8] A.H. Ruhaimi, M.A.A. Aziz, A.A. Jalil, J. CO_2 Util. 43 (2021) 101357.
[9] L. Wang, J. Zhang, F. Chen, Micropor. Mesopor. Mat. 122(1) (2009) 229.
[10] B. Abarna, T. Preethi, A. Karunanithi, G. Rajarajeswari, Mater. Sci. Semicond. Process. 56 (2016) 243.
[11] Y. Tang, Z. Li, Z. Xu, J. Zhang, C. Qu, Z. Zhang, RSC Adv. 10(48) (2020) 28695.
[12] J.J. Huang, C.C. Wang, L.T. Jin, F. Chen, Z.G. Chen, Trans. Nonferrous Met. Soc. China 27(3) (2017) 578.
[13] Z. Jia, G. Luo, H. Wu, Z. Li, T. Ni, M. Ai, Solid State Sci. 94 (2019) 120.
[14] S. Taghavi Fardood, A. Ramazani, S. Woo Joo, J. Appl. Chemical Research 12(1) (2018) 8.
[15] D. Ramimoghadam, M.Z.B. Hussein, Y.H. Taufiq-Yap, Chem. Cent. J. 7(1) (2013) 71.
[16] X. Ma, Y. Li, X. Yan, W. Zhang, J. Zhao, Z. Wang, Chem. Eng. J. 361 (2019) 235.
[17] J. Yang, M. Wang, S. Zhao, Y. Liu, W. Zhang, B. Wu, Q. Liu, Int. J. Hydrog. Energy 44(2) (2019) 870.
[18] A. Chen, J. Qian, Y. Chen, X. Lu, F. Wang, Z. Tang, Powder Technol. 249 (2013) 71.
[19] B. Wu, C. Shan, X. Zhang, H. Zhao, S. Ma, Y. Shi, J. Yang, H. Bai, Q. Liu, Appl. Surf. Sci. 543 (2021) 148677.
[20] A.H. Ruhaimi, M.A. Ab Aziz, Chem. Phys. Lett. 779 (2021) 138842.
[21] A.H. Ruhaimi, M.A.A. Aziz, Appl. Phys. A 128(1) (2022) 1.
[22] A.H. Ruhaimi, C.C. Teh, M.A.A. Aziz, Bull. Chem. React. Eng (2021) 16(2), 366.
[23] B. Su, M. Zhong, L. Han, M. Wei, Y. Liu, H. Yang, Z. Lei, Mater. Res. Bull. 124 (2020) 110777.
[24] M.A. Ahsan, M.A. Imam, A.R. Puente Santiago, A. Rodriguez, B. Alvarado-Tenorio, R. Bernal, R. Luque, J.C. Noveron, Green Chem. 22(20) (2020) 6967.
[25] S. Wong, H.H. Tumari, N. Ngadi, N.B. Mohamed, O. Hassan, R. Mat, N.A. Saidina Amin, J. Clean. Prod. 206 (2019) 394.
[26] Y.P. Chen, C.H. Zheng, Y.Y. Huang, Y.R. Chen, Chemosphere 286 (2022) 131770.
[27] M. Nur-E-Alam, M. Abu Sayid Mia, F. Ahmad, M. Mafizur Rahman, Appl. Water Sci. 8(5) (2018) 129.
[28] J.O. Ighalo, A.G. Adeniyi, SN Appl. Sci. 2(3) (2020) 509.
[29] N. Abdullah, N. Osman, S. Hasan, O. Hassan, Int. J. Electrochem. Sci. 7 (2012) 9401.
[30] P. Li, R. Chen, Y. Lin, W. Li, Chem. Eng. J. 404 (2021) 126459.
[31] J.H. Lee, H. Jeon, J.T. Park, J.H. Kim, Biomass Bioenerg. 142 (2020) 105788.
[32] P. Li, Y. Lin, R. Chen, W. Li, Dalton Trans. 49(16) (2020) 518.
[33] Y. Guo, C. Tan, P. Wang, J. Sun, W. Li, C. Zhao, P. Lu, Chem. Eng. J. 379 (2020) 122277.
[34] K. Nemade, S. Waghuley, Int. J. Met. (2014).
[35] A.D. Prasetya, M. Rifai, Mujamilah, H. Miyamoto, J. Phys. Conf. Ser. 1436(1) (2020) 012113.
[36] B. Choudhury, A. Choudhury, Mater. Chem. Phys. 131(3) (2012) 666.
[37] A. Khorsand Zak, W.H. Abd. Majid, M.E. Abrishami, R. Yousefi, Solid State Sci. 13(1) (2011) 251.
[38] K. Maniammal, G. Madhu, V. Biju, Physica E Low Dimens. Syst. Nanostruct. 85 (2017) 214.

[39] K. Igenepo John, A. Abdul Adenle, A. Timothy Adeleye, I. Pearl Onyia, C. Amune-Matthews, M.O. Omorogie, Chem. Phys. Lett. 776 (2021) 138725.
[40] P.M. Shafi, A.C. Bose, AIP Adv. 5(5) (2015) 057137.
[41] K.K. Han, Y. Zhou, W.G. Lin, J.H. Zhu, Micropor. Mesopor. Mat. 169 (2013) 112.
[42] N.C.S. Selvam, R.T. Kumar, L.J. Kennedy, J.J. Vijaya, J. Alloys Compd. 509(41) (2011) 9809.
[43] H. Jeon, Y.J. Min, S.H. Ahn, S.M. Hong, J.S. Shin, J.H. Kim, K.B. Lee, Colloids Surf. A: Physicochem. Eng. Asp. 414 (2012) 75.
[44] I.F. Mironyuk, V.M. Gun'ko, M.O. Povazhnyak, V.I. Zarko, V.M. Chelyadin, R. Leboda, J. Skubiszewska-Zięba, W. Janusz, Appl. Surf. Sci. 252(12) (2006) 4071.
[45] J. Sivasankari, S. Selvakumar, K. Sivaji, S. Sankar, J. Alloys Compd. 616 (2014) 51.
[46] L. Hopkinson, P. Kristova, K. Rutt, G. Cressey, Geochim. Cosmochim. Acta. 76 (2012) 1.
[47] D. Ochs, M. Brause, B. Braun, W. Maus-Friedrichs, V. Kempter, Surf. Sci. 397(1-3) (1998) 101.
[48] I.W. Sutapa, A.W. Wahab, P. Taba, N. La Nafie, Orient. J. Chem. 34(2) (2018) 1016.
[49] S. Aksay, Phys. B: Condens. Matter 570 (2019) 280.
[50] X. Ma, Y. Wu, M. Fang, B. Liu, R. Chen, R. Shi, Q. Wu, Z. Zeng, L. Li, Biomass Bioenerg. 158 (2022) 106353.